

The Simulated Atmospheric Response to Western North Pacific Sea Surface Temperature Anomalies

SIMCHAN YOOK,^a DAVID W. J. THOMPSON,^a LANTAO SUN,^a AND CASEY PATRIZIO^a

^a Department of Atmospheric Science, Colorado State University, Fort Collins, Colorado

(Manuscript received 11 May 2021, in final form 25 January 2022)

ABSTRACT: Observations reveal two distinct patterns of atmospheric variability associated with wintertime variations in midlatitude sea surface temperatures (SSTs) in the North Pacific sector: 1) a pattern of atmospheric circulation anomalies that peaks 2–3 weeks prior to large SST anomalies in the western North Pacific that is consistent with “atmospheric forcing” of the SST field, and 2) a pattern that lags SST anomalies in the western North Pacific by several weeks that is consistent with the “atmospheric response” to the SST field. Here we explore analogous lead–lag relations between the atmospheric circulation and western North Pacific SST anomalies in two sets of simulations run on the NCAR Community Earth System Model version 1 (CESM1): 1) a simulation run on a fully coupled version of CESM1 and 2) a simulation forced with prescribed, time-evolving SST anomalies over the western North Pacific region. Together, the simulations support the interpretation that the observed lead–lag relationships between western North Pacific SST anomalies and the atmospheric circulation reveal the patterns of atmospheric variability that both force and respond to midlatitude SST anomalies. The results provide numerical evidence that SST variability over the western North Pacific has a demonstrable effect on the large-scale atmospheric circulation throughout the North Pacific sector.

KEYWORDS: Atmosphere-ocean interaction; Atmospheric circulation; Sea surface temperature; North Pacific Ocean

1. Introduction

It is clear that the atmospheric circulation influences sea surface temperature (SST) variability in the midlatitudes. Sea surface temperature variability in the North Atlantic and North Pacific is strongly forced by the atmospheric circulation through the surface heat fluxes and Ekman transport (e.g., Davis 1976; Frankignoul and Hasselmann 1977; Frankignoul 1985; Deser and Timlin 1997; Alexander 2010 and references therein). Circulation variability in the extratropical upper oceans is driven predominantly by variations in the surface wind stress (e.g., Vallis 2017).

It is less clear whether extratropical SST variability, in turn, influences the atmospheric circulation (e.g., Kushnir et al. 2002). Linear theory predicts that the surface fluxes associated with midlatitude SST anomalies are balanced primarily by horizontal temperature advection by the lower-tropospheric flow (Hoskins and Karoly 1981). However, the predicted changes in the atmospheric flow are modest relative to the large internal variability of the extratropical atmosphere, which can complicate the detection of the response (e.g., Kushnir et al. 2002). The atmospheric response is further complicated by its dependence on the mean jet position and feedbacks associated with extratropical wave-mean flow interactions (e.g., Peng et al. 1997; Hall et al. 2001; Peng and Robinson 2001; Kushnir et al. 2002; Woollings et al. 2010; Saulière et al. 2012).

Nevertheless, a growing body of evidence suggest that extratropical SST anomalies can play an active role in climate variability. For example, Czaja and Frankignoul (2002) provide evidence of linkages between North Atlantic SST anomalies

and an atmospheric pattern resembling the North Atlantic Oscillation (NAO). Frankignoul and Sennéchal (2007) and Frankignoul et al. (2011) provide evidence of analogous linkages between North Pacific SST anomalies and large-scale atmospheric variability over the North Pacific sector. A series of studies demonstrate the importance of large SST gradients for the low-level atmospheric flow (e.g., Chelton et al. 2004; O'Neill et al. 2005; Chelton and Xie 2010; Wang et al. 2019). An increasing number of studies reveal seemingly robust linkages between SST anomalies over the Northern Hemisphere western boundary current regions and the free tropospheric flow (e.g., Minobe et al. 2008, 2010; Nakamura et al. 2004, 2008; Xu et al. 2010; Kwon et al. 2010, 2011; Taguchi et al. 2012; Kwon and Joyce 2013; Small et al. 2014b; O'Reilly and Czaja 2015; O'Reilly et al. 2017; Smirnov et al. 2015; Révelard et al. 2016; Wills et al. 2016; Wills and Thompson 2018; Simpson et al. 2019; Athanasiadis et al. 2020; Kwon et al. 2020).

In a pair of recent papers (Wills et al. 2016; Wills and Thompson 2018, hereafter WT18), we argued that the observed lead–lag relationships between the atmospheric circulation and midlatitude SST field uniquely identify the atmospheric circulation anomalies that act to drive and respond to midlatitude SST anomalies. Over both the North Atlantic and North Pacific sectors, the atmospheric circulation anomalies that lead large SST anomalies by several weeks are consistent with horizontal temperature advection anomalies that force the SST field, whereas the atmospheric circulation anomalies that lag large SST anomalies are reminiscent of the linear atmospheric response to midlatitude SST anomalies (Hoskins and Karoly 1981).

The purpose of this study is to 1) test the reproducibility of the observed lead–lag relationships between the midlatitude SST field and atmospheric circulation in output from a fully

Corresponding author: Simchan Yook, simchan.yook@colostate.edu

coupled atmosphere–ocean general circulation model (AOGCM) and 2) test the hypothesis that the lead–lag relationships uniquely reveal the extratropical atmospheric response to midlatitude SST anomalies in a prescribed-SST, Atmospheric Model Intercomparison Project (AMIP)-style simulation. We focus here on atmosphere–ocean interactions over the North Pacific sector. The North Atlantic sector will be considered in a separate study.

2. Data and analysis details

a. Observations

We use two primary observational data sources. The [Hurrell et al. \(2008\)](#) SST dataset is used to generate the boundary conditions used to force the “Kuroshio–Oyashio Global Atmosphere” (KOOGA) experiments over the period 1901–2015 (as described below). All other observational data analyses are based on the European Centre for Medium-Range Weather Forecasts reanalysis version 5 over the period 1979–2020 (ERA5; [Hersbach et al. 2020](#)). Note that SSTs from ERA5 are prescribed from observations [see [Hersbach et al. \(2020\)](#) and references therein].

b. Models and experiments

The primary results are based on experiments run on two different configurations of the NCAR Community Earth System Model version 1 (CESM1; [Hurrell et al. 2013](#)): 1) a fully coupled configuration in which SSTs are interactive (the coupled AOGCM experiment) and 2) a prescribed SST configuration in which the model is driven by SST anomalies prescribed over the western North Pacific. The atmospheric component of the model is the Community Atmospheric Model version 5 (CAM5) run with 30 vertical levels. CAM5 is run at horizontal resolution of $0.9^\circ \times 1.25^\circ$ in the fully coupled configuration and $1.9^\circ \times 2.5^\circ$ in the prescribed SST configuration. The ocean component of the model is run on the CESM nominal 1° horizontal resolution grid.

The coupled simulations run on CESM1 include 40 members of a large ensemble integrated with historical forcings over the period 1920–2005 and representative concentration pathway 8.5 (RCP8.5) forcing from 2006 to 2100 ([Kay et al. 2015](#)). We used output from the Coupled AOGCM experiments over the period 1980–2020. The large-ensemble outputs are available through the Large Ensemble Community Project and produced on resources provided by NSF/CISL/Yellowstone. The use of multiple ensemble members in the analyses helps isolate the signatures of atmosphere–ocean interactions from other forms of internal climate variability.

The prescribed SST experiments are forced with 1) time-varying SST anomalies in the western North Pacific region over an area corresponding roughly to the Kuroshio–Oyashio Extension (KOE) region and 2) the annually repeating seasonal cycle of SSTs over all other regions of the World Ocean. As such, the experiments isolate the influence of SST anomalies in a particular region—here the western North Pacific—from the influence of SST anomalies over other regions of the globe. The experiment design is analogous to the “middle latitude ocean-

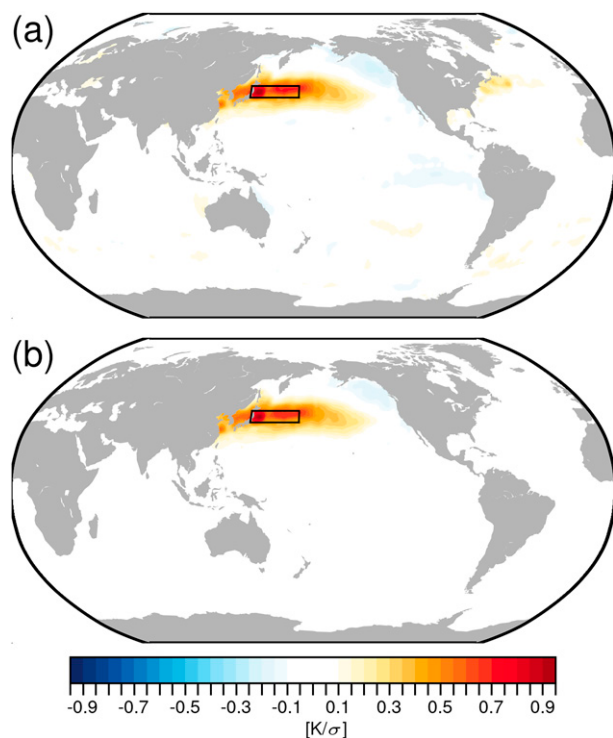


FIG. 1. (top) SST anomalies regressed on standardized SST anomalies averaged over the western North Pacific region (as indicated by the black box). (bottom) The $K_{\text{SST}}^*(x,t)$ pattern used to force the KOOGA simulation. The pattern is identical to that in the top panel, except that SST anomalies outside the North Pacific region are set to zero. See text for details.

global atmosphere” (MOGA) experiments from [Lau and Nath \(1994\)](#). It is also similar to the pacemaker experiments in [Kosaka and Xie \(2013\)](#) but here SST anomalies outside the “pacemaking” region are prescribed to their seasonally varying climatological values rather than coupled.

The pattern of SST anomalies used to force the KOOGA runs is found as follows.

- 1) The linear trend and seasonal cycle is subtracted from SSTs at all grid boxes in the [Hurrell et al. \(2008\)](#) dataset over the period of 1901–2015.
- 2) Variations in SST anomalies over the western North Pacific are defined as the time series of detrended SST anomalies averaged over 36° – 42°N , 140° – 171°E (as indicated by the box in Fig. 1a), which corresponds to the region of largest variance in the North Pacific SST field and roughly to the Kuroshio–Oyashio Extension region. The time series is hereafter denoted as the K index time series $K(t)$, where t denotes the month.
- 3) The pattern of wintertime SST anomalies associated with variations in $K(t)$ is found by regressing December–February (DJF) SST anomalies onto standardized values of $K(t)$. The resulting regression map is shown in the top panel of Fig. 1 and is hereafter denoted $\beta_{\text{KSST}}(x)$, where x denotes the grid point.
- 4) Sea surface temperature anomalies at all months 1901–2015 are decomposed into two components: (i) a component that

- is linearly congruent with the pattern of $\beta_{\text{KSST}}(x)$ [hereafter $\beta_{\text{KSST}}^*(x, t)$] and (ii) a component that is linearly independent of $\beta_{\text{KSST}}(x)$. Note that at that time step i , $\beta_{\text{KSST}}^*(x, i)$ has the same spatial structure as $\beta_{\text{KSST}}(x)$ but amplitude determined by the spatial projection of $\beta_{\text{KSST}}(x)$ onto the SST data at time step i .
- 5) The amplitude of $\beta_{\text{KSST}}(x)$ [and thus $\beta_{\text{KSST}}^*(x, t)$] is very weak outside the western North Pacific (Fig. 1a). Nevertheless, to ensure SST anomalies outside the North Pacific do not influence the model response, we set all values in $\beta_{\text{KSST}}^*(x, t)$ to zero outside the region $5^\circ\text{--}65^\circ\text{N}$, $115^\circ\text{E}\text{--}115^\circ\text{W}$. An 11° running average is applied at the boundary of the region to avoid any discontinuities in the SST field. The resulting pattern is shown in the bottom of Fig. 1.
- 6) The global SST boundary forcing used in the KOGA experiments is formed by adding (i) the matrix of time-varying SST anomalies given by $\beta_{\text{KSST}}^*(x, t)$ and (ii) the annually repeating, climatological-mean seasonal cycle of SSTs. As such, the experiment is forced by the time-varying evolution of the pattern shown in the bottom panel of Fig. 1 superposed on the annually repeating climatological-mean SST field.

The KOGA simulations are integrated over the period 1901–2015. The experiments were repeated five times to yield a total sample size of 575 years.

The KOGA results are also compared with output from a global ocean–global atmosphere (GOGA) AMIP-style experiment forced with prescribed time-varying SSTs from across the globe. The GOGA experiments were run on NCAR CAM5 with a horizontal resolution of $0.9^\circ \times 1.25^\circ$. SSTs and sea ice were derived from ERSSTv4 and HadISST1. We analyze 10 ensemble members run over the period 1880–2014. The GOGA runs were conducted by the NCAR Climate Variability and Change Working Group and are available from the NCAR Climate Data Gateway.

c. Analysis details

Anomalies are defined as deviations from the long-term mean annual cycle. All observations are linearly detrended to remove the influence of trends on the results. Sea level pressure (SLP) is expressed as geopotential height at 1000 hPa (Z_{100}). Area averages are weighted by pressure and cosine of latitude as necessary. Lag regression analyses are centered on DJF, so results at, for example, lag -1 indicate monthly values for November–January regressed on monthly values for December–February.

For the KOGA and GOGA simulations, the regression analyses are conducted first for individual ensemble members and then the resulting regression coefficients are averaged over all ensembles. The results based on the KOGA simulations are thus derived from $5 \text{ ensemble members} \times 115 \text{ years per ensemble} \times 3 \text{ months per year} = 1725 \text{ time steps}$. For the coupled AOGCM simulations, the regression analyses are conducted for output concatenated from all 40 ensemble members and thus over 4920 time steps (40 ensemble members $\times 41 \text{ years per ensemble} \times 3 \text{ months per year}$).

Statistical significance for key results is shown in the appendix in Figs. A1 and A2. The significance of a regression coefficient

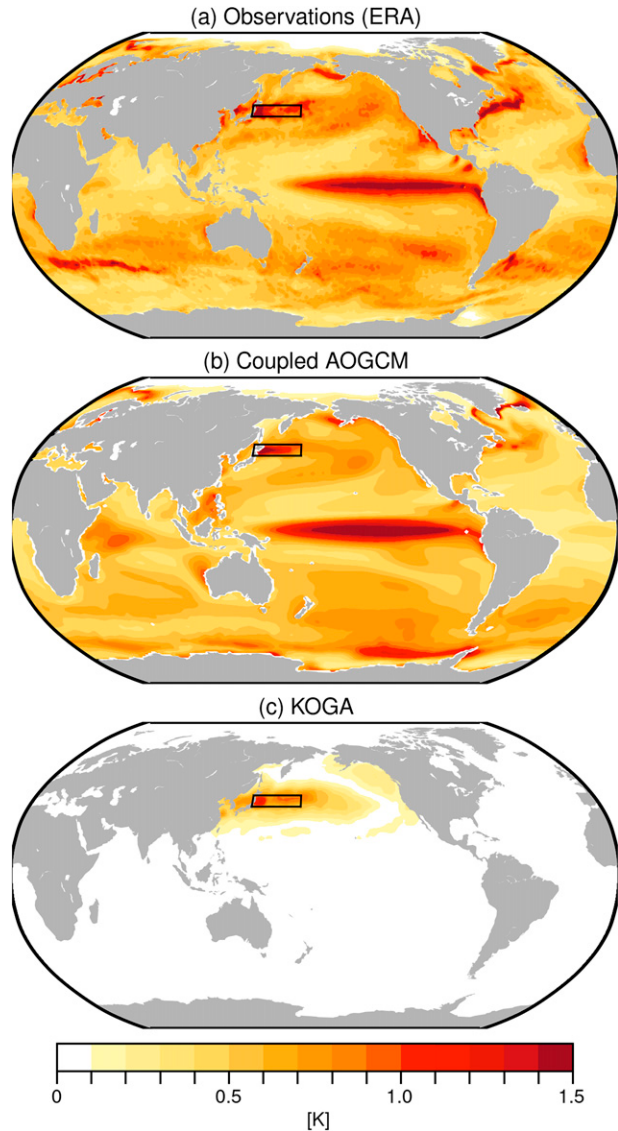


FIG. 2. Standard deviations of the SST anomaly field in (a) observations (ERA5 over 1979–2020), (b) the coupled AOGCM (CESM1), and (c) the KOGA experiment.

is assessed by 1) applying Student's t statistic to the associated correlation coefficient r and 2) assuming

$$n \frac{1 - r_1 r_2}{1 + r_1 r_2}$$

degrees of freedom, where n is the number of time steps, and r_1 and r_2 are the lag-1 autocorrelations of the time series being correlated (Bretherton et al. 1999).

3. Results

Figure 2 shows the standard deviations of the SST field derived from observations (i.e., ERA5), the coupled simulation, and the KOGA simulation. Note that the standard deviations

in Figs. 2b and 2c are found for individual ensemble members and then averaged over all ensembles. The ERA5 SSTs are constrained by observations (Hersbach et al. 2020) and indicate that the regions of largest SST variances are located in the eastern tropical Pacific and in the Kuroshio, Gulf Stream, and Agulhas Return Current regions (Fig. 2a). The coupled AOGCM (Fig. 2b) reproduces broadly the pattern of observed SST variances, although there are differences in the amplitude and structure of the SST variances over regions of large variance, including the western North Pacific. These differences are discussed more below. The variances from the KOGA experiment (Fig. 2c) arise from the time evolution of the $\beta_{\text{KSST}}^*(x, t)$ pattern and are by construction centered on the North Pacific region.

In the rest of this section, we explore the lead-lag relationships between SST variability over the North Pacific and the large-scale atmospheric circulation in the observations and both numerical configurations. The basis for the lag regressions is the K index time series, which as noted in section 2 is defined as standardized values of detrended SST anomalies averaged over the western North Pacific (black boxes in Fig. 2). The K index time series is normalized by the spatially averaged SST variability over the KOE region for all months. We begin with lag regressions derived from the observations.

The top row of Fig. 3 shows the lag regressions of ERA5 SLP (contours) and SSTs (shading) onto the ERA5 K index time series. The lags range from -1 month (left column) to $+1$ month (right column). The results are a reproduction of the key finding from WT18 but for monthly mean data. By construction, the largest SST anomalies are found in the western North Pacific in the vicinity of the Kuroshio–Oyashio Extension region. The SST anomalies are very similar at all lags, consistent with the persistence of the SST field. In contrast, the atmospheric circulation anomalies change notably from one lag to the next. The month prior to peak positive anomalies in KOE region is marked by positive SLP anomalies that span much of the North Pacific basin (Fig. 3, top left); the month following peak positive anomalies in the KOE region is marked by low SLP anomalies that overlie and extend downstream of the KOE region (Fig. 3, top right). The primary SLP anomalies in both patterns are statistically significant (see Fig. A1 in the appendix).

For completeness, results for lags extending from lag -3 to $+5$ are shown in Fig. A3. The region of positive SLP anomalies at negative lag is evident as early as lag -3 but peaks in amplitude at lag -1 months. The region of low SLP anomalies at positive lag is apparent at lag $+2$ but shrinks notably beyond that.

The atmospheric anomalies at negative lag are consistent with anomalously warm advection over the region of large SST gradients in the Kuroshio–Oyashio Extension region (see also Deser and Timlin 1997; Ciausto and Thompson 2004; WT18). The SLP anomalies at negative lag are thus consistent with atmospheric forcing of the SST field. In contrast, the atmospheric anomalies at positive lag indicate anomalously cold advection over the western North Pacific. They are thus consistent with the linear atmospheric response to the SST field, in which the surface fluxes associated with SST anomalies are balanced by horizontal temperature advection

(Hoskins and Karoly 1981). The maximum amplitude of the anomalies at positive lag is about ~ 12 m in Z_{1000} (1.5 hPa in SLP) per standard deviation of the K index time series in observations. These amplitudes correspond to roughly 7% (27%) of the variance (standard deviation) of the observed January–March SLP variability near the low pressure center of action in the western North Pacific (not shown).

The interpretation of the SLP pattern at positive lag as the atmospheric “response” is supported by the projection of the attendant surface turbulent heat flux anomalies onto the SST anomalies. Figure 4 (top) shows the product of 1) the surface fluxes of sensible and latent heat regressed onto the K index and 2) the SST anomalies in Fig. 3 (top). Note that multiplying the fluxes and SST anomalies emphasizes regions where the fluxes contribute to the SST anomalies of interest; results not weighted by the SST anomalies are shown in Fig. A4. Regions where the product is positive indicate areas where the SST anomalies are reinforced by the surface fluxes; regions where the product is negative indicate areas where the SST anomalies are damped by the surface fluxes. As evidenced in the figure, the period prior to peak SST anomalies is associated with warming of the ocean mixed layer by the atmosphere, whereas the period following peak SST anomalies is associated with warming of the atmosphere by the ocean.

Interestingly, the lag 0 regression map can be viewed as the linear superposition of the forcing (lag -1) and response (lag $+1$) patterns. To see this, the bottom two rows of Fig. 3 show the decomposition of the SLP lag-regression maps into the so-called forcing pattern and a component linearly independent of the forcing pattern. The decomposition is done as follows: 1) The forcing pattern is defined as the SLP regression map at lag -1 month (Fig. 3, top left). 2) The amplitude of the forcing pattern is found at each lag as the (spatial) regression of the respective SLP regression map onto the forcing pattern. This yields the component of the SLP regression map that is linearly congruent with the forcing pattern at each lag. 3) Finally, the residual “response” patterns are found by subtracting the linearly congruent component of the forcing pattern from the SLP regression maps.

The decomposition is shown in the second and third rows of Fig. 3 and highlights two key results:

- 1) The forcing pattern accounts for the entirety of the total regression map at lag -1 , by construction (Fig. 3, left column). But its amplitude decreases with lag and is negligible at lag $+1$ (middle row). Thus the full regression maps at lag -1 (top left) and lag $+1$ (top right) are effectively linearly independent of each other.
- 2) The residual regression maps are very similar at lag 0 and lag $+1$, despite the fact they are not constrained to be so. Thus the residual patterns are largely dominated by a single structure, and the lag regressions in the top row can be viewed as the time-varying linear superposition of two distinct structures.

Figure 5 explores the corresponding lead-lag relationships in the coupled AOGCM model output. As noted earlier, the

Regressions onto western North Pacific SSTs: Observations

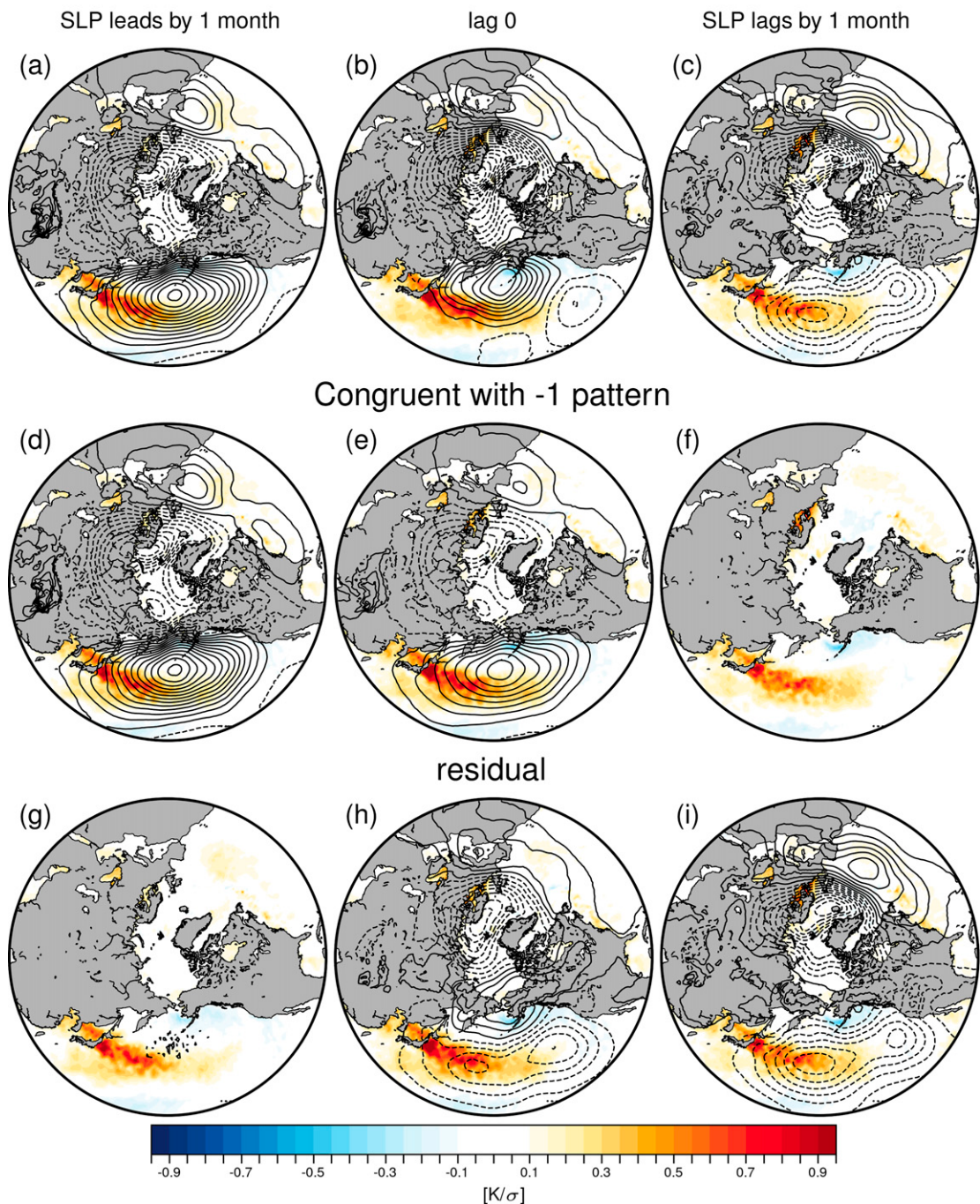


FIG. 3. (a)–(c) Observed wintertime lag regressions of the SST and Z_{1000} fields onto standardized values of the K index time series. Negative lags denote Z_{1000} and SST anomalies lead the K index time series, and vice versa. (d)–(f) As in (a)–(c), but the Z_{1000} contours show the components of the Z_{1000} regression coefficients that are linearly congruent with the pattern in (a). (g)–(i) As in (d)–(f), but the Z_{1000} contours show the differences between the Z_{1000} anomalies in (a)–(c) and (d)–(f). The SST field is indicated by shading, and the Z_{1000} field is indicated by contours. Solid (dashed) contours indicate positive (negative) anomalies. The Z_{1000} contours are spaced at 2-m intervals starting at ± 1 m. The same contour intervals are used in other figures throughout the paper except where otherwise noted.

Regressions onto western North Pacific SSTs

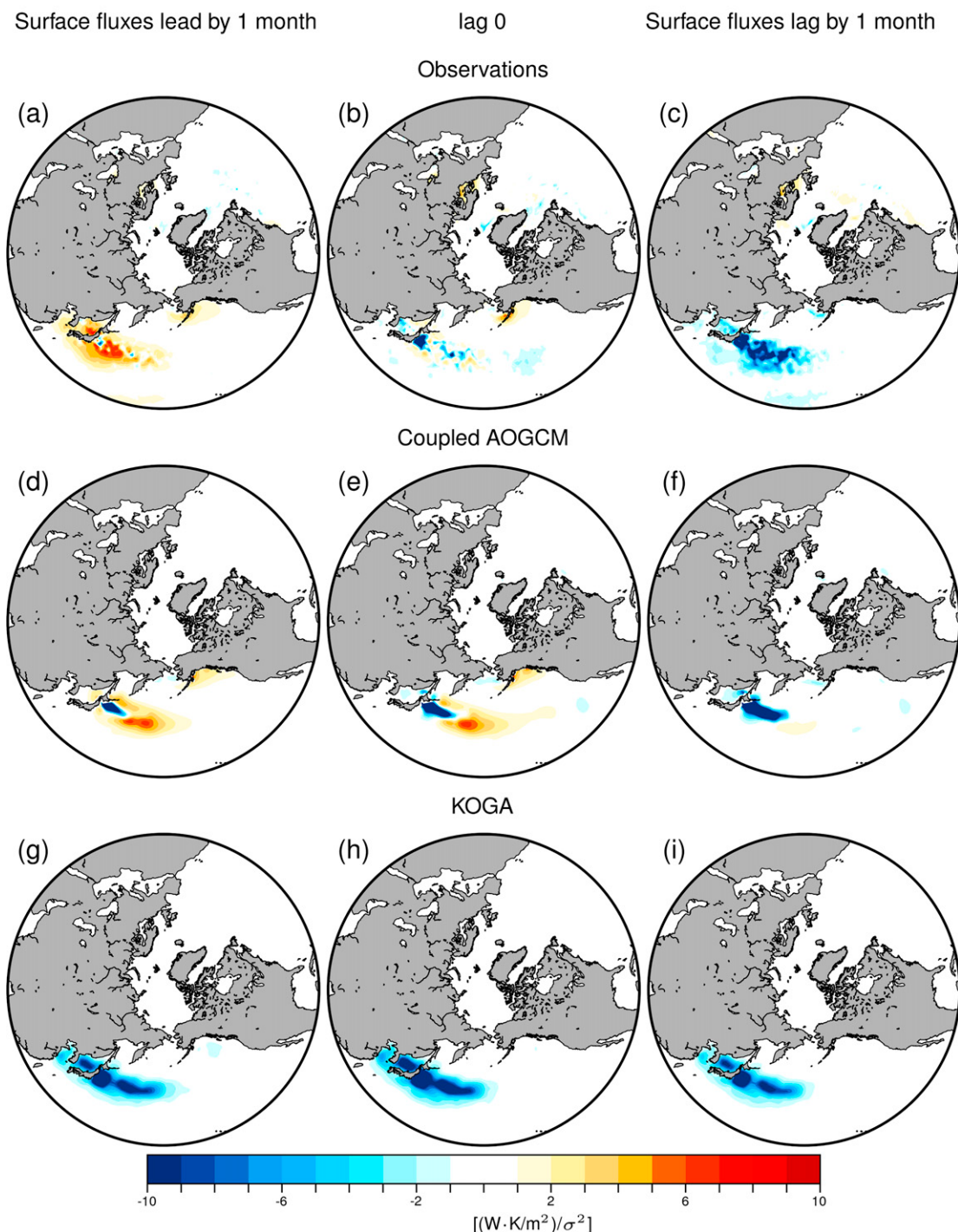


FIG. 4. The product of 1) the surface fluxes of sensible and latent heat and 2) SSTs regressed onto the K index time series. Results are shown for (a)–(c) observations, (d)–(f) the coupled AOGCM output, and (g)–(i) the KOGA output. Regions where the product is positive (negative) indicate areas where the SST anomalies are reinforced (damped) by the surface fluxes.

Regressions onto western North Pacific SSTs: Coupled AOGCM

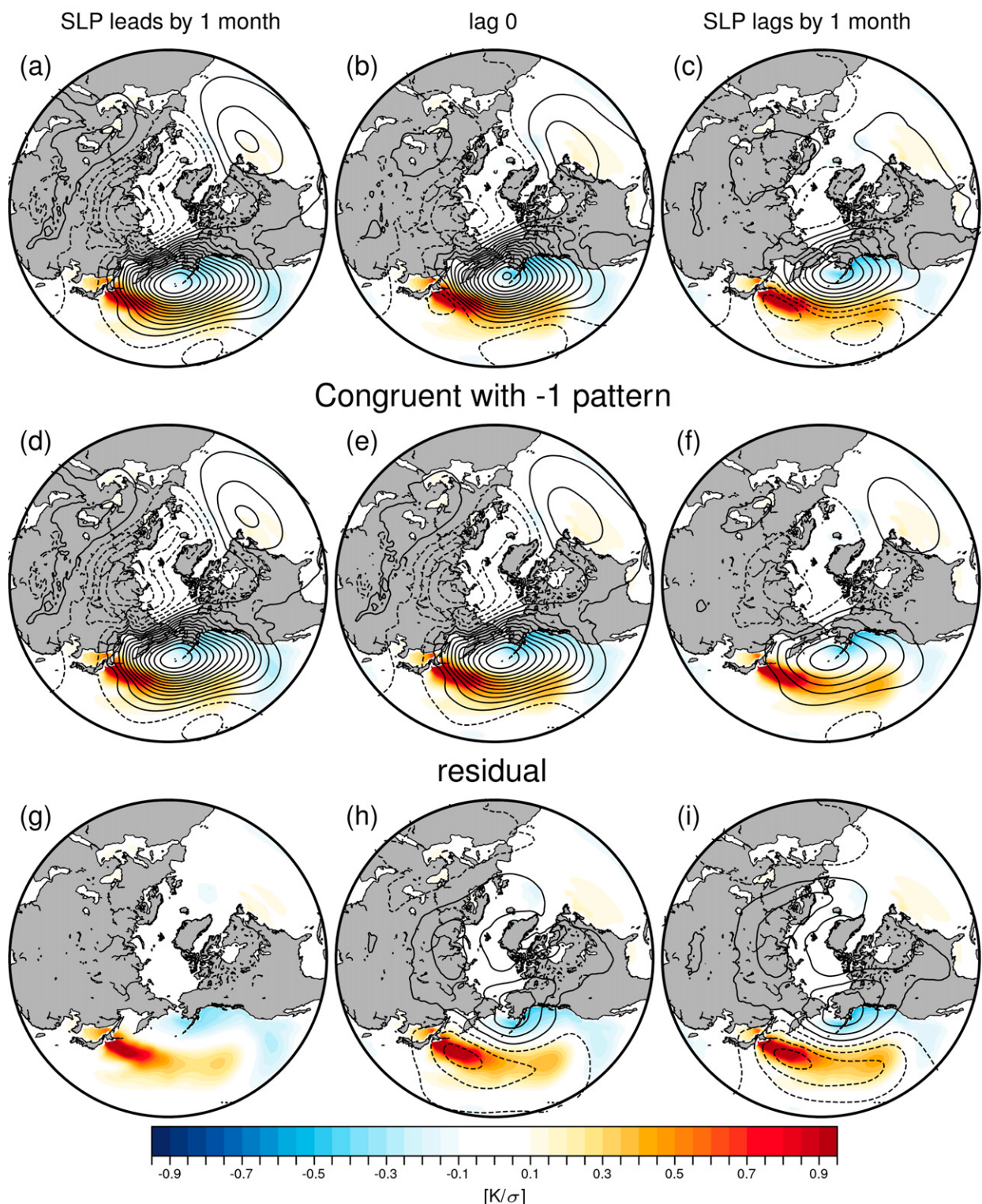


FIG. 5. As in Fig. 3, but for output from the coupled AOGCM (CESM1). The Z_{1000} contours are spaced at 2-m intervals starting at ± 1 m.

coupled AOGCM captures well the observed SST variability over most of the globe albeit with some differences on the basin scale. There are two prominent differences between the coupled AOGCM output and the observations over the North Pacific SST field: 1) The largest SST variability in the western North Pacific in the AOGCM is located a few degrees poleward of the observational maximum (cf. Figs. 2a,b; see also Small et al. 2019; Thompson and Kwon 2010). For this reason, the K index time series for the coupled AOGCM is based on SSTs averaged over a region shifted 3 degrees poleward of that used for the observations (as indicated by the box in Fig. 2b). 2) The SST variances in the western North Pacific are slightly larger in the AOGCM than they are in the observations. For example, the standard deviations of SSTs averaged over the K index time series region for the DJF period (i.e., the standard deviations of the K index time series) are 0.82 K in the AOGCM output and 0.73 K in the observations, and the averages of the grid point standard deviations over the same region are ~ 1.0 K in the coupled AOGCM and 0.85 K in the observations. The larger variances in the coupled AOGCM output are consistent with biases in the model SST response to both oceanic (Thompson and Kwon 2010) and atmospheric processes (Small et al. 2019; Small et al. 2020). Neither of these differences qualitatively affect the results of the regressions (not shown).

The lag -1 regression map derived from the coupled AOGCM (Fig. 5, top left) is qualitatively similar to that derived from observations (Fig. 3, top left). Both are dominated by statistically significant SLP anomalies consistent with northward flow and thus warm temperature advection over the region of large SST gradients in the Kuroshio–Oyashio Extension region (significance is shown in Fig. A1).

The lag $+1$ regression map derived from the coupled AOGCM (Fig. 5, top right) also bears similarity to its observational counterpart (Fig. 3, top right) in that both exhibit negative SLP anomalies across the North Pacific. However, it also exhibits notable differences; in particular, the coupled AOGCM map exhibits positive SLP anomalies over the Bering Sea that are not apparent in the observations. The decomposition of the coupled model results into a “forcing” (Fig. 5, middle row) and residual (Fig. 5, bottom row) pattern—as done for observations in Fig. 3—reveals that the differences between the observed and coupled AOGCM lag $+1$ regression maps derive not from differences in the response pattern, but rather from differences in the persistence of the forcing pattern. Comparing the middle rows of Figs. 3 and 5, it is clear that the forcing pattern persists much longer in the coupled AOGCM than it does in observations. When the projection of the forcing pattern is removed from the coupled AOGCM regression maps (Fig. 5, bottom), the residual pattern is more clearly dominated by low SLP anomalies that span the central North Pacific and increase in amplitude with lag.

The enhanced persistence of the forcing pattern in the coupled AOGCM potentially derives from model biases in the persistence of SLP variability in the North Pacific sector. The enhanced persistence of the forcing pattern, in turn, leads to enhanced persistence of the corresponding SST anomalies. The longer time scale of SST anomalies in the western North

Pacific in the coupled AOGCM is apparent in Fig. A3; the longer time scale of SLP anomalies is evidenced in the differences in the lag-1 autocorrelations of SLP averaged over the North Pacific sector bounded by 35° – 70° N, 150° E– 130° W: the lag 1 month autocorrelation in the coupled AOGCM output is $r \sim 0.3$; the lag 1 month autocorrelations in observations is $r \sim 0.2$.

To leading order, the relative signs of the surface heat fluxes and SST anomalies in the coupled AOGCM are qualitatively similar to those derived from observations (cf. Fig. 4, top and middle rows; see also Fig. A4): The fluxes generally reinforce the SST anomalies at negative lag (as evidenced by warm shading in Fig. 4) but damp the SST anomalies at positive lag (as evidenced by cool shading). Note that regions where the relationship between the surface heat fluxes and SSTs are out of phase—as indicated by the blue shading—are centered primarily over the KOE frontal region, where the air-sea flux variability is driven predominantly by SST variations arising from intrinsic oceanic variability (Small et al. 2019). The AOGCM indicates a small region where the SSTs are damped by the surface fluxes over the KOE region that is not evident in the observations (see the small region of blue shading near the coast of Japan), which suggests the CESM overestimates the contribution of oceanic processes to SST variability in this region.

Together the results in Figs. 3–5 indicate the following:

- 1) Lag regressions between the SLP field and SSTs averaged over the western North Pacific consist of two distinct patterns: (i) a pattern consistent with *forcing* of SST anomalies over the KOE region by horizontal atmospheric temperature advection that peaks at negative lag; and (ii) a pattern consistent with *damping* of SST anomalies over the KOE region by horizontal atmospheric temperature advection that peaks at positive lag and is consistent with the linear atmospheric response to midlatitude SST anomalies. The response pattern is most clear when the component of the regressions that is linearly congruent with the forcing is subtracted from the lag regression maps (Figs. 3 and 5, bottom)
- 2) Results based on both observations and coupled model output are very similar. The primary differences derive from the persistence of the model “forcing” pattern, which exhibits larger persistence than its observational counterpart, and thus partially obscures the coupled model response pattern at positive lag (Fig. 5, right column).

To what extent is the atmospheric response—as inferred from the results in the bottom-right panels of Fig. 3 and 5—recovered in the experiment forced with the time history of SST anomalies over the western North Pacific? Figure 6 is constructed in the same manner as the top rows of Figs. 3 and 5, but shows results based on the KOGA simulation. Recall that the KOGA simulation is forced by the climatological-mean, seasonal cycle of SSTs throughout the globe superposed on the time evolution of the pattern of SST anomalies shown in Fig. 1. Note that the regression coefficients based on the KOGA output are calculated first for individual ensemble members and then averaged over all ensembles. Thus the amplitudes can be compared directly with the observations and coupled model output.

Regressions onto western North Pacific SSTs: KOGA experiment

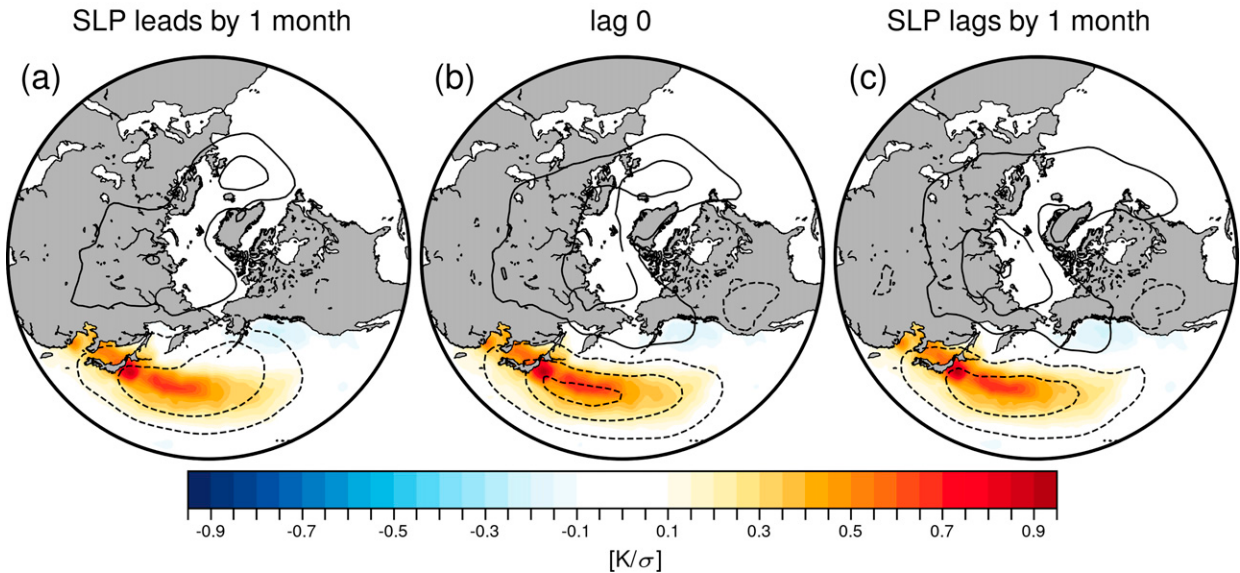


FIG. 6. As in Figs. 3a–c, but for output from the KOGA simulation. The Z_{1000} contours are spaced at 2-m intervals starting at ± 1 m.

The KOGA results do not exhibit a distinct atmospheric forcing pattern at negative lag (i.e., they do not exhibit a pattern consistent with warm advection over the western North Pacific). This is expected, since the model is forced with prescribed SST anomalies, and thus horizontal temperature advection by the

atmosphere is incapable of influencing the SST field. Rather, the KOGA results indicate a pattern consistent with the atmospheric response at all lags. In other words, at all lags the KOGA output indicates 1) heat fluxes that act to damp the SST field and thus warm the lower atmosphere (Fig. 4,

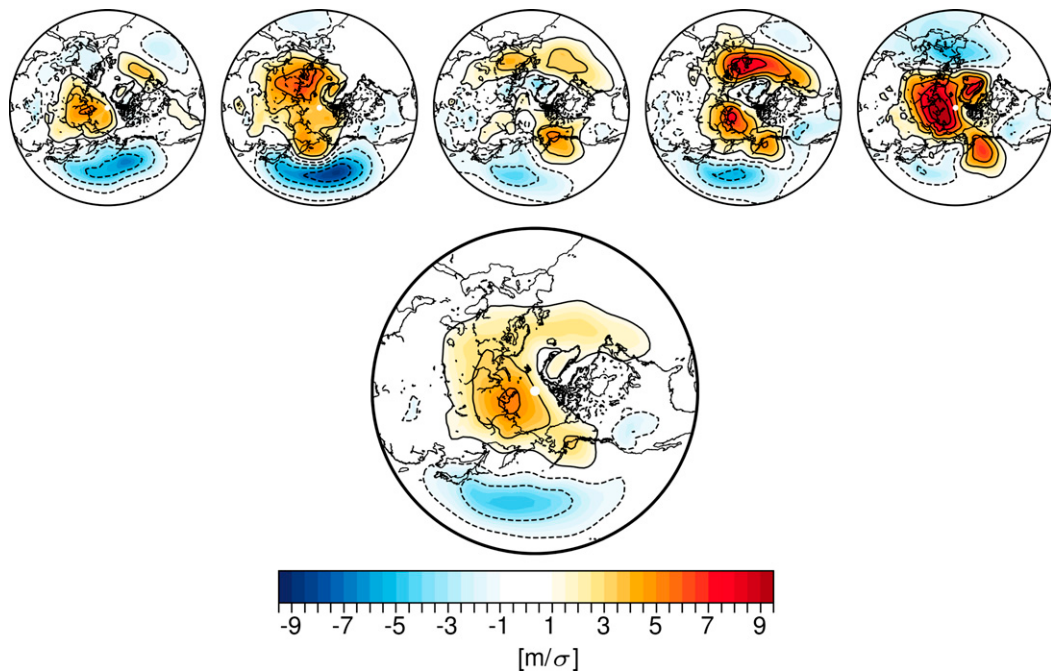


FIG. 7. (top) Wintertime lag regressions of the Z_{1000} field onto the K index time series at lag +1 from each ensemble member in the KOGA run. (bottom) The ensemble-mean lag +1 regression coefficients from the KOGA run reproduced from the contours in Fig. 6c. Shading and contours both indicate the Z_{1000} field.

Regressions onto western North Pacific SSTs at lag +1 month

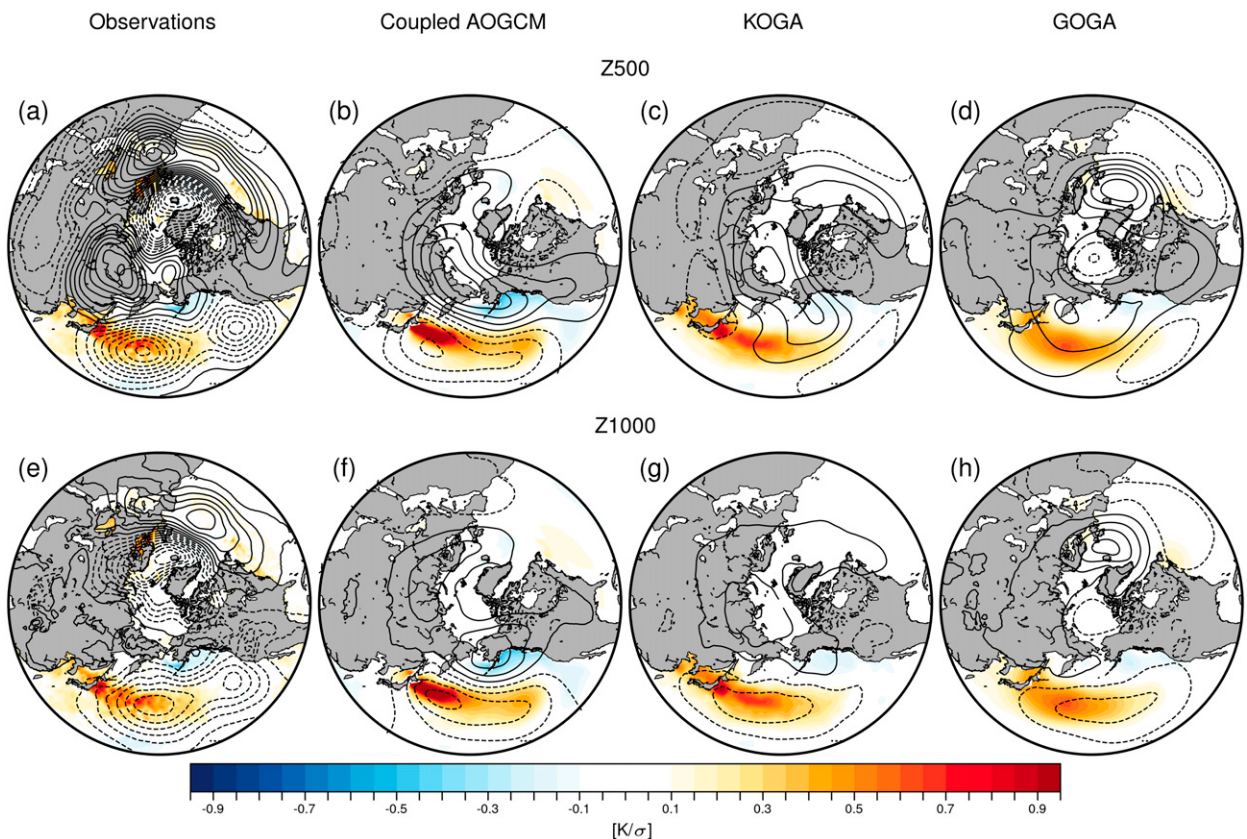


FIG. 8. (e)–(h) Wintertime lag regressions of the Z_{1000} and SST fields onto the K index time series lag +1 based on observations, the coupled AOGCM (CESM1), the KOGA, and the GOGA experiment. The Z_{1000} results in (e) and (f) show the components of the regression coefficients that are linearly unrelated to the lag −1 regressions; that is, they show the “residual” regression coefficients reproduced from Figs. 3i and 5i, respectively. (a)–(d) As in (e)–(h), but for results based on the Z_{500} field. The Z_{1000} and Z_{500} contours are spaced at 2-m intervals starting at ± 1 m.

bottom) and 2) SLP anomalies consistent with cold advection over the western North Pacific (Fig. 6) that act to balance the surface fluxes.

The close similarity between the atmospheric response in the KOGA simulation (Fig. 6) and the inferred atmospheric response from observations (Fig. 3i) suggests that the latter reflects the observed atmospheric response to SST anomalies over the western North Pacific. In both the KOGA simulation and observations, the low-level circulation anomalies are consistent with the linear, balanced response to extratropical SST anomalies; that is, the surface low is shifted to the east of warm SST anomalies so that horizontal temperature advection over the Kuroshio–Oyashio Extension region acts to oppose the anomalous fluxes of heat into the lower atmosphere and thus damp the underlying SST anomaly.

The response in the KOGA experiments is highly reproducible and significant. The regression coefficients in the primary center of action are significant based on the t statistic (Fig. A1). The low pressure center of action varies in amplitude from one ensemble member to the next, but its

primary center over the western half of the North Pacific is reproducible in all five ensemble members (Fig. 7). Importantly, the response is consistent with the observational and coupled model results shown in Figs. 3 and 5 (bottom right). The amplitude of the KOGA SLP anomalies is somewhat less than the amplitude of the residual SLP anomalies from observations and the coupled AOGCM output (cf. Fig. 6, right, with Figs. 3 and 5, bottom right). But the general patterns of the observed, coupled AOGCM, and KOGA SLP anomalies are all clearly very similar to each other.

Figure 8 probes the vertical structure of the responses. The bottom row reproduces the responses in Z_{1000} from the observations, coupled AOGCM, KOGA, and GOGA experiments. That is, the figure shows the lag +1 results reproduced from (first column) the observations from Fig. 3i, (second column) the coupled AOGCM output from Fig. 5i, (third column) the KOGA output from Fig. 6c, and (fourth column) the GOGA output. The top row shows the same results but for results based on the Z_{500} field. The Z_{500} regression coefficients in Figs. 8a and 8b were calculated in the same way as

those in the bottom-right panels of Figs. 3 and 5; that is, they are the differences between the Z_{500} lag +1 regression maps and the components that are linearly congruent with the Z_{500} lag -1 regression maps.

The circulation anomalies derived from the KOGA output (right column) peak in the lower troposphere, again consistent with the linear baroclinic response to extratropical SST anomalies (Hoskins and Karoly 1981; Kushnir et al. 2002). However, in contrast, the circulation anomalies derived from observations and the coupled AOGCM output (left and middle columns) exhibit equivalent barotropic structures with more pronounced anomalies aloft.

Why do the observations and coupled AOGCM indicate an equivalent barotropic response while the KOGA output indicates a shallow response? One possibility is that the upper-tropospheric anomalies in the observations and coupled AOGCM arise from SST anomalies that lie outside the western North Pacific, such as the tropical Pacific. We view this as unlikely for two reasons: 1) SST anomalies regressed on the K index time series do not exhibit notable amplitude outside the North Pacific (Fig. A5) and 2) analogous results formed from AMIP-style experiments forced with SST anomalies across the globe (the GOGA runs described in section 2) also do not reveal notable anomalies aloft (Fig. 8d). The similarity between results derived from the GOGA and KOGA simulations suggests that SST anomalies in the KOE region dominate the results from the GOGA output.

A second possibility is that the upper-level response is muted in the KOGA run due to insufficient horizontal resolution. Previous studies have shown that high horizontal resolution is required to correctly represent the coupling between mesoscale ocean eddies and the extratropical atmospheric circulation (Czaja et al. 2019; Ma et al. 2015, 2017; Smirnov et al. 2015; Small et al. 2014a, 2019; Siqueira and Kirtman 2016) and that it also leads to a more robust upper-tropospheric response (Smirnov et al. 2015). However, it is notable that the GOGA run has the same horizontal resolution as the coupled AOGCM but nevertheless exhibits a very different response aloft.

A third possibility is that the upper-level response is influenced by the temporal resolution of the SST boundary conditions. For example, Zhou et al. (2015) argue that daily fluctuations in the SST field play an important role in generating a realistic simulation of the large-scale atmospheric response. The SST boundary conditions in the KOGA run include monthly mean SST values linearly interpolated to the daily time scale. They thus lack realistic variability on submonthly time scales.

A fourth possibility is that the upper-level response evident in the observations and coupled AOGCM is dependent on two-way coupling between the atmosphere and SST field. This could be tested by conducting experiments analogous to the KOGA simulation but where we prescribe time-varying anomalous fluxes of heat in the ocean mixed layer in the KOE region rather than the SST field itself, thus permitting thermodynamic coupling at the sea surface.

It would be interesting to explore the sensitivity of the atmospheric response in KOGA-like experiments run at different horizontal resolutions, realistic daily variations in the SST field, and forced with prescribed ocean heat fluxes

rather than prescribed SSTs (i.e., as in Kwon et al. 2011). These experiments are deferred to a future study.

4. Discussion and conclusions

Extratropical atmosphere–ocean interactions potentially play a crucial role in climate variability. But key aspects of such interactions remain poorly understood. In part, this is because the linear response to midlatitude SST anomalies is expected to be small relative to the noise inherent in the midlatitude circulation (Hoskins and Karoly 1981) and the total response is likely to include difficult to predict nonlinear changes in atmospheric eddies (Kushnir et al. 2002).

In a recent study (WT18) we argued that the lead–lag relationships between the extratropical circulation and the SST field uniquely identify two structures associated with SST variability in the western North Pacific: 1) a pattern that leads SST variability and is consistent with forcing of the SST field by the atmospheric circulation and 2) a pattern that lags SST variability and is consistent with the linear atmospheric response to extratropical SST anomalies (Hoskins and Karoly 1981). Lead–lag regressions alone do not prove causality. But the close correspondence between the lagged response and that expected from linear theory strongly suggests that it reflects the atmospheric response to SST anomalies. The results in WT18 build on a growing body of evidence that SST anomalies in the western boundary current regions can have a demonstrable effect on the tropospheric circulation (see discussion and references in section 1).

Here we tested 1) the reproducibility of the observed lead–lag relationships from WT18 in output from a fully coupled AOGCM and 2) the reproducibility of the observed lagged circulation anomalies in a prescribed SST AMIP-style simulation. The key findings are the following:

- 1) The observed characteristics of atmosphere–ocean coupling in the North Pacific are well captured by the coupled AOGCM. Periods of anomalously high SSTs in the western North Pacific are preceded by circulation and heat flux anomalies that are consistent with atmospheric forcing of the SST field, and followed by circulation and heat flux anomalies that are consistent with the atmospheric response to the SST field.
- 2) The low-level component of the “response” pattern inferred from lag regressions in observations and the coupled AOGCM is recovered in numerical experiments forced with the time history of western North Pacific SST anomalies (the KOGA experiment).
- 3) The low-level component of the response pattern is highly robust in observations, the coupled AOGCM, and in the prescribed SST experiment (the KOGA experiment). In the latter case, the response pattern emerges not only in the ensemble mean but in most individual ensemble members.

One notable difference between results derived from the observations and coupled AOGCM relative to those derived from the KOGA simulation is the vertical structure of the response. The inferred responses from the observations and the coupled AOGCM have a deep

Regressions onto western North Pacific SSTs

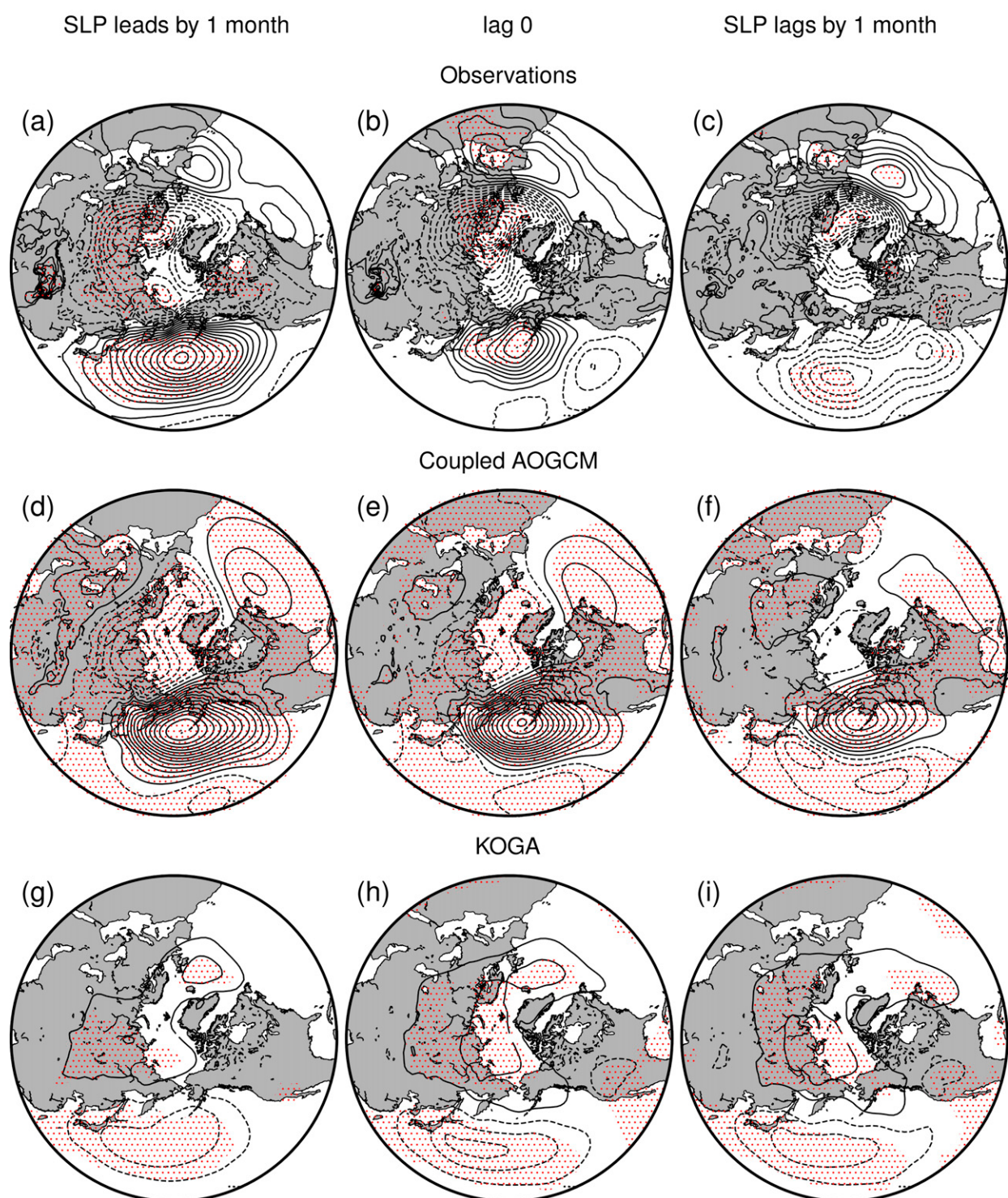


FIG. A1. Z_{1000} regression coefficients reproduced from the top rows in Figs. 3, 5, and 6. Stippling indicates regions where the significance of the attendant correlation coefficients are significant at the 95% level. See text for details.

Regressions onto western North Pacific SSTs at lag +1 month

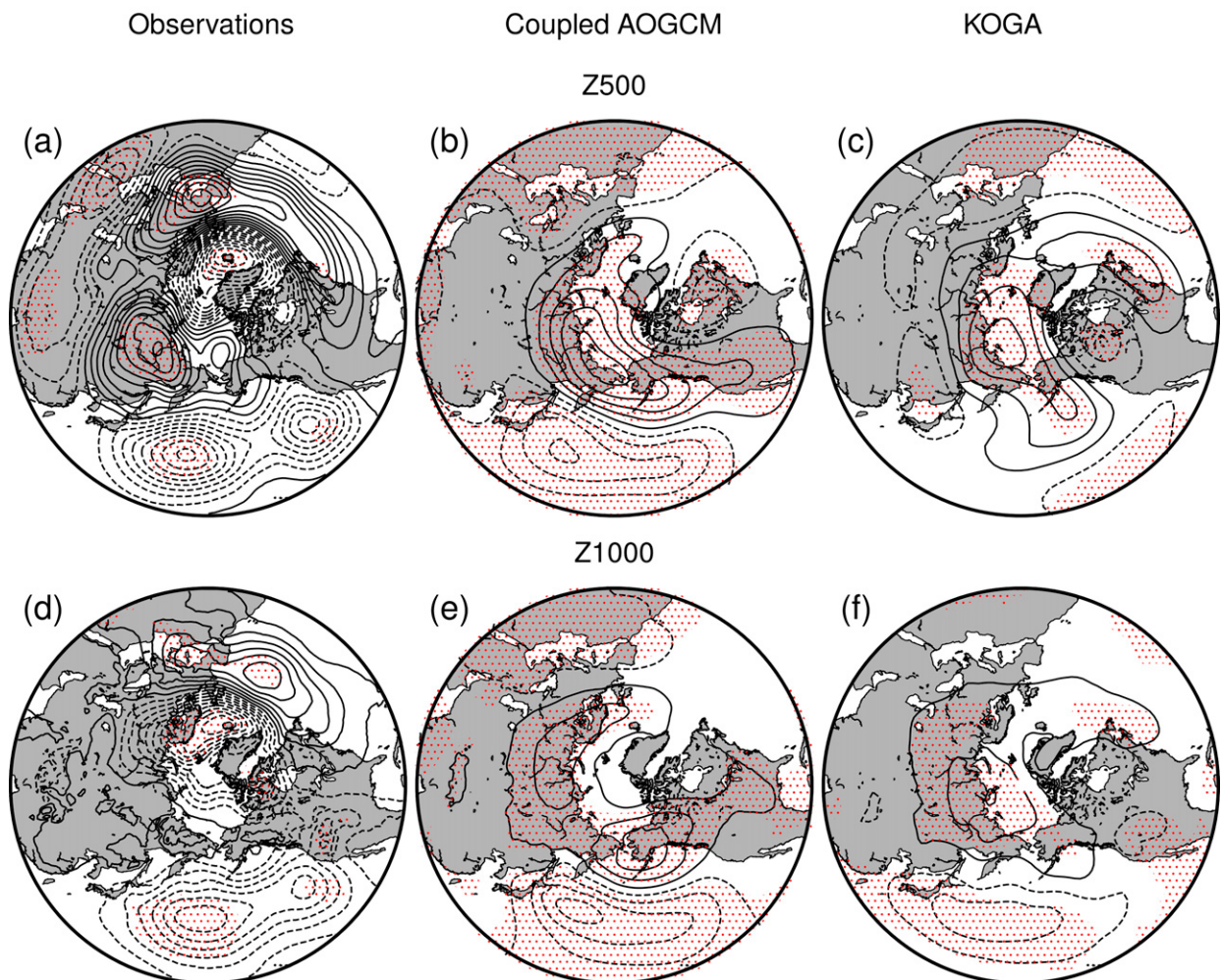


FIG. A2. As in Fig. 8, but with stippling indicating regions where the attendant correlation coefficients exceed the 95% significance level.

equivalent barotropic component, whereas the response in the KOGA simulation is largest in the lower troposphere. We have speculated that the differences in the upper-level responses may derive from a range of factors, including differences in the horizontal resolution of the simulations, the amplitude of day-to-day variability in the SST field, and the representation of coupling between the atmosphere and SST field. These factors will be explored in a future study.

The *near-surface* response to KOE SST anomalies identified here is consistent with the linear response to SST anomalies predicted by linear theory (Hoskins and Karoly 1981) and that found in numerous previous numerical studies [e.g., Kwon et al. 2011; Smirnov et al. 2015; see also the discussion in Kushnir et al. (2002)]. The inconsistency in the *upper-level response* found here is reminiscent of the inconsistency of the upper-level response found in previous studies. For example, many early studies found an equivalent

barotropic response to midlatitude SST anomalies (e.g., see Table 1 in Kushnir et al. 2002). But the structure of the upper-level response has proven sensitive to various aspects of the simulation. The upper-level responses explored in Peng et al. (1997), Peng and Whitaker (1999), and Peng and Robinson (2001) are dependent on the model climatology and patterns of internal variability. The upper-level response in Kwon et al. (2011) appears to be influenced by tropical–extratropical coupling. The upper-level response in Smirnov et al. (2015) varies depending on the model resolution. And the upper-level response in Ma et al. (2015, 2017) is strongly dependent on mesoscale features in the SST field.

Previous studies have suggested that the extratropical atmospheric response to midlatitude SST anomalies is a function of the seasonally varying background flow (e.g., Peng and Whitaker 1999; Taguchi et al. 2012). The simulated

pattern of low-level SLP anomalies found here does not vary notably in results stratified by calendar month (not shown). However, the *observed* lag 1 regressions exhibit a more wavelike structure in data restricted to March (not shown). It is unclear whether the differences between results for March and those for other months are due to variations in the climatological flow or sampling variability. Previous studies have also made clear the caveats associated with forcing an atmospheric GCM with the time history of prescribed SSTs (e.g., Bretherton and Battisti 2000). It is not clear how those caveats would influence the lead–lag relationships that are the focus here. Importantly, the amplitude of the ensemble-mean lagged response is reproducible in individual ensemble members (Fig. 7).

Together, the results shown here suggest that the pattern identified in lead–lag regressions between the atmospheric circulation and the western North Pacific SST field reflects the atmospheric response to SST anomalies in the broad Kuroshio–Oyashio Extension region.

Acknowledgments. The authors thank three anonymous reviewers for their helpful comments on the manuscript. D.W.J.T. and S.Y. are funded by the NSF Climate and Large-Scale Dynamics program. We thank Samantha Wills for discussions of the results. The CESM project is supported by the NSF and the Office of Science (BER) of the U.S. Department of Energy (DOE). The authors acknowledge the Climate Simulation Laboratory at NCAR’s Computational and Information Systems Laboratory (CISL; sponsored by NSF and other agencies) and the NOAA Research and Development High Performance Computing Program for providing computing and storage resources that have contributed to the research results reported within this paper.

APPENDIX

Additional Figures

a. Statistical significance

Figures A1 and A2 show results from the top rows in Figs. 3, 5, and 6 (Fig. A1) and from Fig. 8 (Fig. A2) superposed with stippling where the significance of the results exceeds the 95% level. See section 2 for details of the calculation of significance.

b. Results for lags beyond -1 to $+1$ month

Figure A3 shows the same results as Fig. 3 (top), Fig. 5 (top), and Fig. 6, but extends the results to additional lags ranging from -3 to $+5$ months.

c. Surface fluxes

Figure A4 shows the observed turbulent fluxes of heat regressed onto the K index time series.

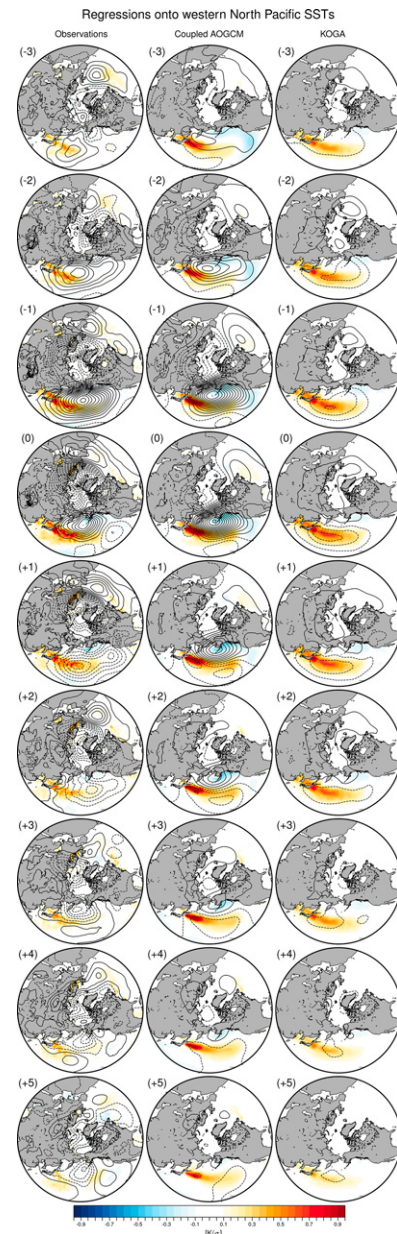


FIG. A3. The evolution of the SST and Z_{1000} fields regressed onto the K -SST index in (left) the observations, (center) the coupled AOGCMs, and (right) the KOGA runs. The Z_{1000} contours are spaced at 2-m intervals starting at ± 1 m.

d. Global SST anomalies associated with the K index time series

Figure A5 shows SSTs regressed on the K index time series for the global domain.

Regressions onto western North Pacific SSTs

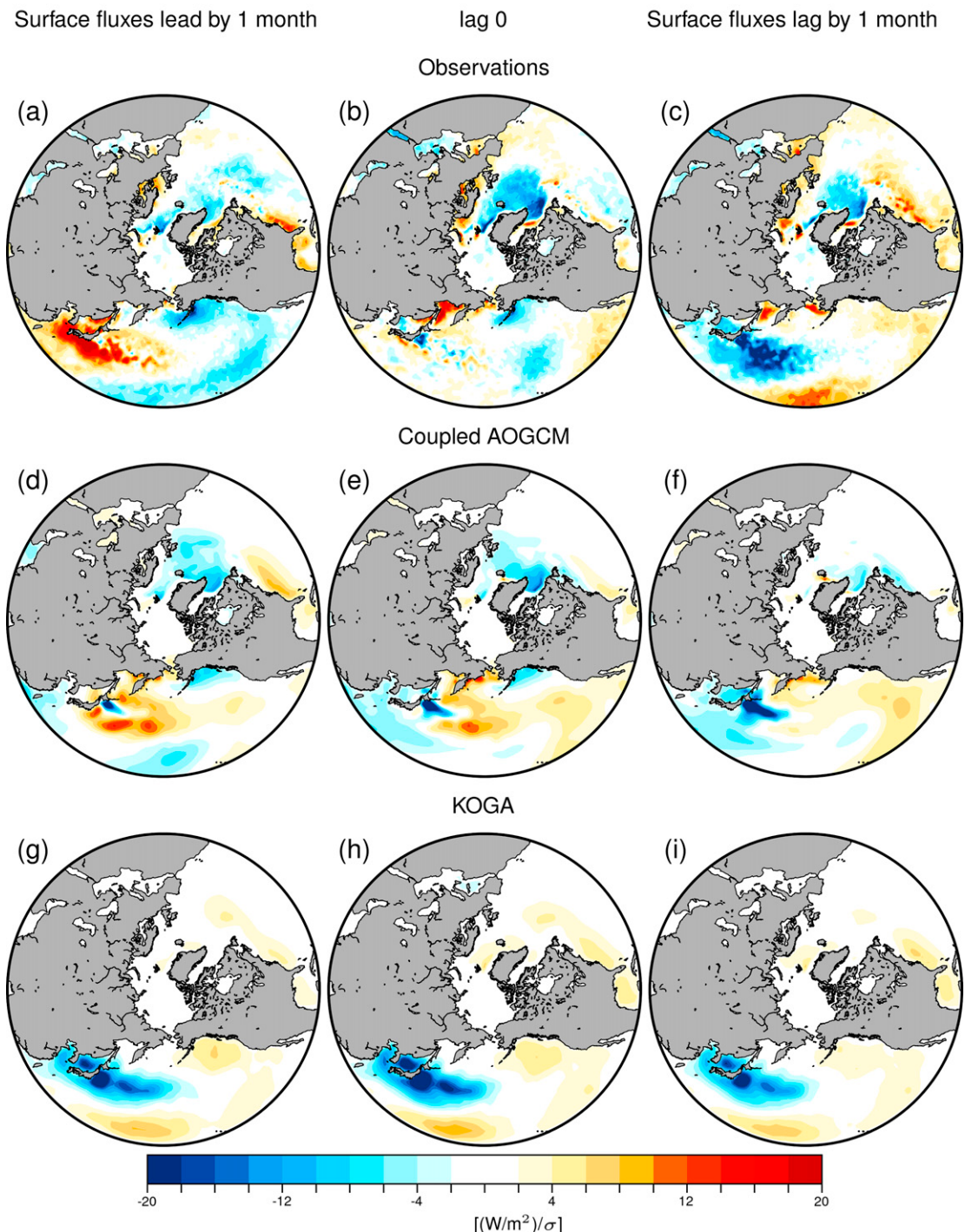


FIG. A4. The surface fluxes of sensible and latent heat regressed onto the K index time series. Results are shown for (a)–(c) observations, (d)–(f) the coupled AOGCM output, and (g)–(i) the KOGA output. Regions where the fluxes are positive (negative) indicate areas where surface fluxes are into the ocean (atmosphere).

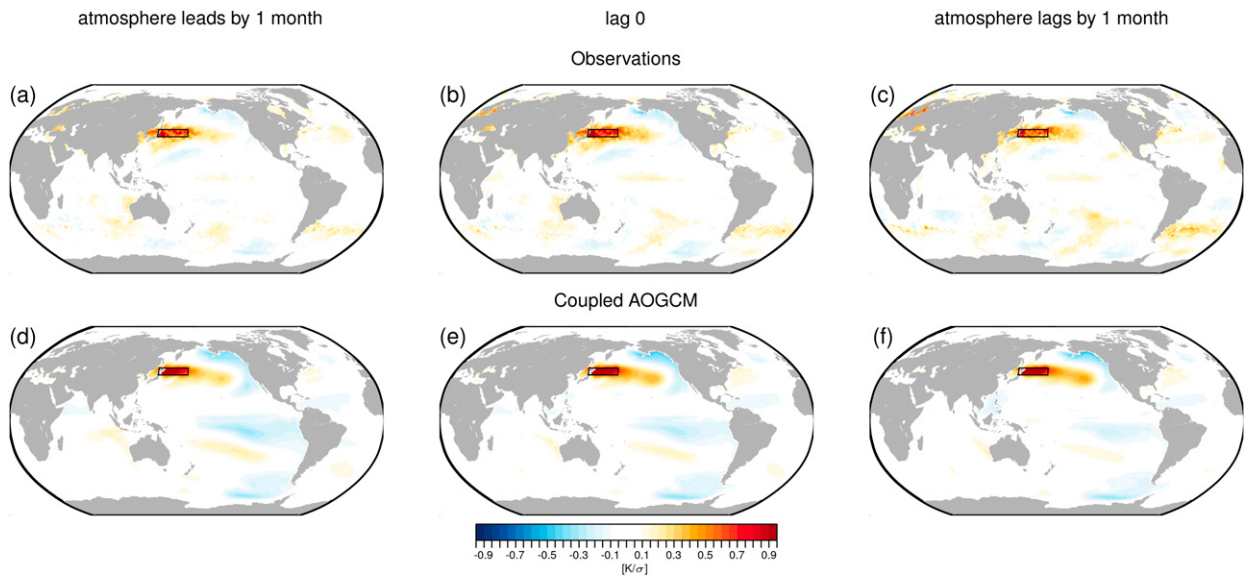


FIG. A5. As in the SST anomalies from Figs. 3a–c, but for the global domain; i.e., results show SST anomalies regressed on the K index based on (a)–(c) observations and (d)–(f) the coupled AOGCM.

REFERENCES

- Alexander, M., 2010: Extratropical air-sea interaction, sea surface temperature variability, and the Pacific decadal oscillation. *Climate Dynamics: Why Does Climate Vary? Geophys. Monogr.*, Vol. 123, Amer. Geophys. Union, 148 pp.
- Athanasiadis, P. J., S. Yeager, Y.-O. Kwon, A. Bellucci, D. W. Smith, and S. Tibaldi, 2020: Decadal predictability of North Atlantic blocking and the NAO. *npj Climate Atmos. Sci.*, **3**, 20, <https://doi.org/10.1038/s41612-020-0120-6>.
- Bretherton, C. S., and D. S. Battisti, 2000: An interpretation of the results from atmospheric general circulation models forced by the time history of the observed sea surface temperature distribution. *Geophys. Res. Lett.*, **27**, 767–770, <https://doi.org/10.1029/1999GL010910>.
- , M. Widmann, V. P. Dymnikov, J. M. Wallace, and I. Bladé, 1999: The effective number of spatial degrees of freedom of a time-varying field. *J. Climate*, **12**, 1990–2009, [https://doi.org/10.1175/1520-0442\(1999\)012<1990:TENOSD>2.0.CO;2](https://doi.org/10.1175/1520-0442(1999)012<1990:TENOSD>2.0.CO;2).
- Chelton, D. B., and S.-P. Xie, 2010: Coupled ocean-atmosphere interaction at oceanic mesoscales. *Oceanography*, **23**, 52–69, <https://doi.org/10.5670/oceanog.2010.05>.
- , M. Schlax, M. Freilich, and R. Milliff, 2004: Satellite radar measurements reveal short-scale features in the wind stress field over the world ocean. *Science*, **303**, 978–983, <https://doi.org/10.1126/science.1091901>.
- Ciasto, L. M., and D. W. Thompson, 2004: North Atlantic atmosphere-ocean interaction on intraseasonal time scales. *J. Climate*, **17**, 1617–1621, [https://doi.org/10.1175/1520-0442\(2004\)017<1617:NAAOI>2.0.CO;2](https://doi.org/10.1175/1520-0442(2004)017<1617:NAAOI>2.0.CO;2).
- Czaja, A., and C. Frankignoul, 2002: Observed impact of Atlantic SST anomalies on the North Atlantic Oscillation. *J. Climate*, **15**, 606–623, [https://doi.org/10.1175/1520-0442\(2002\)015<0606:OIOASA>2.0.CO;2](https://doi.org/10.1175/1520-0442(2002)015<0606:OIOASA>2.0.CO;2).
- , —, S. Minobe, and B. Vannière, 2019: Simulating the midlatitude atmospheric circulation: What might we gain from high-resolution modeling of air-sea interactions? *Curr. Climate Change Rep.*, **5**, 390–406, <https://doi.org/10.1007/s40641-019-00148-5>.
- Davis, R. E., 1976: Predictability of sea surface temperature and sea level pressure anomalies over the North Pacific Ocean. *J. Phys. Oceanogr.*, **6**, 249–266, [https://doi.org/10.1175/1520-0485\(1976\)006<0249:POSSTA>2.0.CO;2](https://doi.org/10.1175/1520-0485(1976)006<0249:POSSTA>2.0.CO;2).
- Deser, C., and M. S. Timlin, 1997: Atmosphere-ocean interaction on weekly timescales in the North Atlantic and Pacific. *J. Climate*, **10**, 393–408, [https://doi.org/10.1175/1520-0442\(1997\)010<0393:AOIOWT>2.0.CO;2](https://doi.org/10.1175/1520-0442(1997)010<0393:AOIOWT>2.0.CO;2).
- Frankignoul, C., 1985: Sea surface temperature anomalies, planetary waves, and air-sea feedback in the middle latitudes. *Rev. Geophys.*, **23**, 357–390, <https://doi.org/10.1029/RG023i004p00357>.
- , and K. Hasselmann, 1977: Stochastic climate models, Part II Application to sea-surface temperature anomalies and thermocline variability. *Tellus*, **29**, 289–305, <https://doi.org/10.3402/tellusa.v29i4.11362>.
- , and N. Sennéchal, 2007: Observed influence of North Pacific SST anomalies on the atmospheric circulation. *J. Climate*, **20**, 592–606, <https://doi.org/10.1175/JCLI4021.1>.
- , —, Y.-O. Kwon, and M. A. Alexander, 2011: Influence of the meridional shifts of the Kuroshio and the Oyashio Extensions on the atmospheric circulation. *J. Climate*, **24**, 762–777, <https://doi.org/10.1175/2010JCLI3731.1>.
- Hall, N. M., J. Derome, and H. Lin, 2001: The extratropical signal generated by a midlatitude SST anomaly. Part I: Sensitivity at equilibrium. *J. Climate*, **14**, 2035–2053, [https://doi.org/10.1175/1520-0442\(2001\)014<2035:TESGBA>2.0.CO;2](https://doi.org/10.1175/1520-0442(2001)014<2035:TESGBA>2.0.CO;2).
- Hersbach, H., and Coauthors, 2020: The ERA5 global reanalysis. *Quart. J. Roy. Meteor. Soc.*, **146**, 1999–2049, <https://doi.org/10.1002/qj.3803>.
- Hoskins, B. J., and D. J. Karoly, 1981: The steady linear response of a spherical atmosphere to thermal and orographic forcing.

- J. Atmos. Sci.*, **38**, 1179–1196, [https://doi.org/10.1175/1520-0469\(1981\)038<1179:TSLROA>2.0.CO;2](https://doi.org/10.1175/1520-0469(1981)038<1179:TSLROA>2.0.CO;2).
- Hurrell, J. W., J. J. Hack, D. Shea, J. M. Caron, and J. Rosinski, 2008: A new sea surface temperature and sea ice boundary dataset for the Community Atmosphere Model. *J. Climate*, **21**, 5145–5153, <https://doi.org/10.1175/2008JCLI2292.1>.
- , —, and Coauthors, 2013: The Community Earth System Model: A framework for collaborative research. *Bull. Amer. Meteor. Soc.*, **94**, 1339–1360, <https://doi.org/10.1175/BAMS-D-12-00121.1>.
- Kay, J. E., and Coauthors, 2015: The Community Earth System Model (CESM) large ensemble project: A community resource for studying climate change in the presence of internal climate variability. *Bull. Amer. Meteor. Soc.*, **96**, 1333–1349, <https://doi.org/10.1175/BAMS-D-13-00255.1>.
- Kosaka, Y., and S.-P. Xie, 2013: Recent global-warming hiatus tied to equatorial Pacific surface cooling. *Nature*, **501**, 403–407, <https://doi.org/10.1038/nature12534>.
- Kushnir, Y., W. Robinson, I. Bladé, N. Hall, S. Peng, and R. Sutton, 2002: Atmospheric GCM response to extratropical SST anomalies: Synthesis and evaluation. *J. Climate*, **15**, 2233–2256, [https://doi.org/10.1175/1520-0442\(2002\)015<2233:AGRTE>2.0.CO;2](https://doi.org/10.1175/1520-0442(2002)015<2233:AGRTE>2.0.CO;2).
- Kwon, Y.-O., and T. M. Joyce, 2013: Northern Hemisphere winter atmospheric transient eddy heat fluxes and the Gulf Stream and Kuroshio–Oyashio Extension variability. *J. Climate*, **26**, 9839–9859, <https://doi.org/10.1175/JCLI-D-12-00647.1>.
- , M. A. Alexander, N. A. Bond, C. Frankignoul, H. Nakamura, B. Qiu, and L. A. Thompson, 2010: Role of the Gulf Stream and Kuroshio–Oyashio systems in large-scale atmosphere–ocean interaction: A review. *J. Climate*, **23**, 3249–3281, <https://doi.org/10.1175/2010JCLI3343.1>.
- , C. Deser, and C. Cassou, 2011: Coupled atmosphere–mixed layer ocean response to ocean heat flux convergence along the Kuroshio Current Extension. *Climate Dyn.*, **36**, 2295–2312, <https://doi.org/10.1007/s00382-010-0764-8>.
- , H. Seo, C. C. Ummenhofer, and T. M. Joyce, 2020: Impact of multidecadal variability in Atlantic SST on winter atmospheric blocking. *J. Climate*, **33**, 867–892, <https://doi.org/10.1175/JCLI-D-19-0324.1>.
- Lau, N.-C., and M. J. Nath, 1994: A modeling study of the relative roles of tropical and extratropical SST anomalies in the variability of the global atmosphere–ocean system. *J. Climate*, **7**, 1184–1207, [https://doi.org/10.1175/1520-0442\(1994\)007<1184:AMSOR>2.0.CO;2](https://doi.org/10.1175/1520-0442(1994)007<1184:AMSOR>2.0.CO;2).
- Ma, X., and Coauthors, 2015: Distant influence of Kuroshio eddies on North Pacific weather patterns? *Sci. Rep.*, **5**, 17785, <https://doi.org/10.1038/srep17785>.
- , P. Chang, R. Saravanan, R. Montuoro, H. Nakamura, D. Wu, X. Lin, and L. Wu, 2017: Importance of resolving Kuroshio front and eddy influence in simulating the North Pacific storm track. *J. Climate*, **30**, 1861–1880, <https://doi.org/10.1175/JCLI-D-16-0154.1>.
- Minobe, S., A. Kuwano-Yoshida, N. Komori, S.-P. Xie, and R. J. Small, 2008: Influence of the Gulf Stream on the troposphere. *Nature*, **452**, 206–209, <https://doi.org/10.1038/nature06690>.
- , M. Miyashita, A. Kuwano-Yoshida, H. Tokinaga, and S.-P. Xie, 2010: Atmospheric response to the Gulf Stream: Seasonal variations. *J. Climate*, **23**, 3699–3719, <https://doi.org/10.1175/2010JCLI3359.1>.
- Nakamura, H., T. Sampe, Y. Tanimoto, and A. Shimpo, 2004: Observed associations among storm tracks, jet streams and midlatitude oceanic fronts. *Earth's Climate: The Ocean–Atmosphere Interaction. Geophys. Monogr.*, Vol. 147, 329–345.
- , —, A. Goto, W. Ohfuchi, and S.-P. Xie, 2008: On the importance of midlatitude oceanic frontal zones for the mean state and dominant variability in the tropospheric circulation. *Geophys. Res. Lett.*, **35**, L15709, <https://doi.org/10.1029/2008GL034010>.
- O'Neill, L. W., D. B. Chelton, S. K. Esbensen, and F. J. Wentz, 2005: High-resolution satellite measurements of the atmospheric boundary layer response to SST variations along the Agulhas Return Current. *J. Climate*, **18**, 2706–2723, <https://doi.org/10.1175/JCLI3415.1>.
- O'Reilly, C. H., and A. Czaja, 2015: The response of the Pacific storm track and atmospheric circulation to Kuroshio Extension variability. *Quart. J. Roy. Meteor. Soc.*, **141**, 52–66, <https://doi.org/10.1002/qj.2334>.
- , S. Minobe, A. Kuwano-Yoshida, and T. Woollings, 2017: The Gulf Stream influence on wintertime North Atlantic jet variability. *Quart. J. Roy. Meteor. Soc.*, **143**, 173–183, <https://doi.org/10.1002/qj.2907>.
- Peng, S., and J. S. Whitaker, 1999: Mechanisms determining the atmospheric response to midlatitude SST anomalies. *J. Climate*, **12**, 1393–1408, [https://doi.org/10.1175/1520-0442\(1999\)012<1393:MDTART>2.0.CO;2](https://doi.org/10.1175/1520-0442(1999)012<1393:MDTART>2.0.CO;2).
- , —, and W. A. Robinson, 2001: Relationships between atmospheric internal variability and the responses to an extratropical SST anomaly. *J. Climate*, **14**, 2943–2959, [https://doi.org/10.1175/1520-0442\(2001\)014<2943:RBAIVA>2.0.CO;2](https://doi.org/10.1175/1520-0442(2001)014<2943:RBAIVA>2.0.CO;2).
- , —, and M. P. Hoerling, 1997: The modeled atmospheric response to midlatitude SST anomalies and its dependence on background circulation states. *J. Climate*, **10**, 971–987, [https://doi.org/10.1175/1520-0442\(1997\)010<0971:TMARTM>2.0.CO;2](https://doi.org/10.1175/1520-0442(1997)010<0971:TMARTM>2.0.CO;2).
- Révelard, A., C. Frankignoul, N. Sennéchal, Y.-O. Kwon, and B. Qiu, 2016: Influence of the decadal variability of the Kuroshio Extension on the atmospheric circulation in the cold season. *J. Climate*, **29**, 2123–2144, <https://doi.org/10.1175/JCLI-D-15-0511.1>.
- Saulière, J., D. J. Brayshaw, B. Hoskins, and M. Blackburn, 2012: Further investigation of the impact of idealized continents and SST distributions on the Northern Hemisphere storm tracks. *J. Atmos. Sci.*, **69**, 840–856, <https://doi.org/10.1175/JAS-D-11-0113.1>.
- Simpson, I. R., S. G. Yeager, K. A. McKinnon, and C. Deser, 2019: Decadal predictability of late winter precipitation in Western Europe through an ocean–jet stream connection. *Nat. Geosci.*, **12**, 613–619, <https://doi.org/10.1038/s41561-019-0391-x>.
- Siqueira, L., and B. P. Kirtman, 2016: Atlantic near-term climate variability and the role of a resolved Gulf Stream. *Geophys. Res. Lett.*, **43**, 3964–3972, <https://doi.org/10.1002/2016GL068694>.
- Small, R. J., and Coauthors, 2014a: A new synoptic scale resolving global climate simulation using the Community Earth System Model. *J. Adv. Model. Earth Syst.*, **6**, 1065–1094, <https://doi.org/10.1002/2014MS000363>.
- , R. A. Tomas, and F. O. Bryan, 2014b: Storm track response to ocean fronts in a global high-resolution climate model. *Climate Dyn.*, **43**, 805–828, <https://doi.org/10.1007/s00382-013-1980-9>.
- , —, —, and S. P. Bishop, 2019: Air–sea turbulent heat fluxes in climate models and observational analyses: What drives their variability? *J. Climate*, **32**, 2397–2421, <https://doi.org/10.1175/JCLI-D-18-0576.1>.

- , F. O. Bryan, S. P. Bishop, S. Larson, and R. A. Tomas, 2020: What drives upper-ocean temperature variability in coupled climate models and observations? *J. Climate*, **33**, 577–596, <https://doi.org/10.1175/JCLI-D-19-0295.1>.
- Smirnov, D., M. Newman, M. A. Alexander, Y.-O. Kwon, and C. Frankignoul, 2015: Investigating the local atmospheric response to a realistic shift in the Oyashio sea surface temperature front. *J. Climate*, **28**, 1126–1147, <https://doi.org/10.1175/JCLI-D-14-00285.1>.
- Taguchi, B., H. Nakamura, M. Nonaka, N. Komori, A. Kuwano-Yoshida, K. Takaya, and A. Goto, 2012: Seasonal evolutions of atmospheric response to decadal SST anomalies in the North Pacific subarctic frontal zone: Observations and a coupled model simulation. *J. Climate*, **25**, 111–139, <https://doi.org/10.1175/JCLI-D-11-00046.1>.
- Thompson, L. A., and Y. Kwon, 2010: An enhancement of low-frequency variability in the Kuroshio–Oyashio extension in CCSM3 owing to ocean model biases. *J. Climate*, **23**, 6221–6233, <https://doi.org/10.1175/2010JCLI3402.1>.
- Vallis, G. K., 2017: *Atmospheric and Oceanic Fluid Dynamics: Fundamentals and Large-Scale Circulation*. Cambridge University Press, 946 pp.
- Wang, Q., S.-P. Zhang, S.-P. Xie, J. R. Norris, J.-X. Sun, and Y.-X. Jiang, 2019: Observed variations of the atmospheric boundary layer and stratocumulus over a warm eddy in the Kuroshio Extension. *Mon. Wea. Rev.*, **147**, 1581–1591, <https://doi.org/10.1175/MWR-D-18-0381.1>.
- Wills, S. M., and D. W. Thompson, 2018: On the observed relationships between wintertime variability in Kuroshio–Oyashio Extension sea surface temperatures and the atmospheric circulation over the North Pacific. *J. Climate*, **31**, 4669–4681, <https://doi.org/10.1175/JCLI-D-17-0343.1>.
- , —, and L. M. Ciasto, 2016: On the observed relationships between variability in Gulf Stream sea surface temperatures and the atmospheric circulation over the North Atlantic. *J. Climate*, **29**, 3719–3730, <https://doi.org/10.1175/JCLI-D-15-0820.1>.
- Woollings, T., B. Hoskins, M. Blackburn, D. Hassell, and K. Hodges, 2010: Storm track sensitivity to sea surface temperature resolution in a regional atmosphere model. *Climate Dyn.*, **35**, 341–353, <https://doi.org/10.1007/s00382-009-0554-3>.
- Xu, H., H. Tokinaga, and S.-P. Xie, 2010: Atmospheric effects of the Kuroshio large meander during 2004–05. *J. Climate*, **23**, 4704–4715, <https://doi.org/10.1175/2010JCLI3267.1>.
- Zhou, G., M. Latif, R. J. Greatbatch, and W. Park, 2015: Atmospheric response to the North Pacific enabled by daily sea surface temperature variability. *Geophys. Res. Lett.*, **42**, 7732–7739, <https://doi.org/10.1002/2015GL065356>.